Experimental investigation of ribbing pattern effect on the bonding qualities of water jet cut steel reinforcement

Architecture, Structures and Construction
https://doi.org/10.1007/s44150-022-00068-3

TECHNICAL NOTE

Experimental investigation of ribbing pattern effect on the bonding qualities of water jet cut steel reinforcement

Rayna Higuchi[1] · **Jackson L. Jewett**[1] · **Josephine V. Carstensen**[1]

Received: 9 June 2022 / Accepted: 11 August 2022

Abstract
With the rise of interest in digital fabrication of reinforced concrete structures, a great number of structural concrete designs that depart from standard prismatic shapes are being suggested. This has prompted an exploration of steel reinforcement strategies that are alternative to the classical deformed or "ribbed" rebars. One such is to cut internal reinforcement from steel plates using a waterjet cutting machine. Advantages of automated waterjet cutting steel reinforcement include high precision and accuracy, and minimal expense for increasing the complexity of (2D) reinforcement layouts. However, it is not known how the application of ribbing patterns along the cut edge of reinforcing bars affects the steel–concrete bond. This work conducts experimental pullout tests of waterjet-cut steel plate reinforcement with three different ribbing patterns and compares the bond strength with equivalent classic rebars. Two of the tested geometries averaged within 90–91% of the pull-out force of conventional rebar, demonstrating viability of this alternative reinforcement method.

Keywords Waterjet · Ribbed geometry · Reinforced concrete · Bond strength · Alternative reinforcement · Experimental testing

Introduction

Digital fabrication is a process in which structures are built with highly precise, computationally controlled machines, rather than manual labor. Examples related to construction include but are not limited to additive manufacturing or 3D printing structural components with steel [1], computer-numerical-controlled (CNC) milling of concrete formwork [2], and robotically mediated placement of masonry blocks [3]. Here, 3D printing refers to the process of placing material layer-by-layer with high precision to build a structure. For many applications, digital fabrication technologies can offer appreciable advantages over traditional methods, such as more rapid construction, precise geometry, efficient material placement, and greater freedom of design [4–6].

Concrete design has received considerable attention in applications of these digital fabrication technologies, likely due to it's ubiquity in the construction industry, and it's highly-formable nature as a structural material. While much of this work has gone into the development of 3D printed concrete (see e.g. review in [7]), many other digital fabrication methods have been applied. Examples include direct extrusion of monolithic concrete members [8], CNC knit flexible formworks [9], and 3D printed formworks for conventional concrete casting [10]. However, although most modern concrete construction relies on integrating internal reinforcing steel (rebar) within the concrete elements, there is not yet consensus on the most effective way to include steel as reinforcement for digitally fabricated concrete (DFC).

Many strategies have been suggested for reinforcing DFC. Asprone et al. [11] offer a thorough review outlining the state of the art on DFC reinforcement with particular emphasis on steel reinforcement strategies for concrete 3D printing. Although reinforcement strategies using fibers or alternative materials merit interest, the discussion in this paper is limited to using larger steel components as the reinforcing phase.

Many reinforcement strategies for DFC rely on the use of conventional rebars. A popular technique is to place traditionally manufactured rebar directly into the concrete member, if the fabrication method allows for it [12, 13]. Equally

✉ Jackson L. Jewett
jljewett@mit.edu

[1] Department of Civil and Environmental Engineering, Massachusetts Institute of Technology, 77 Mass Ave, Cambridge, MA, USA

Published online: 06 September 2022

popular is the strategy of placing rebar or steel tendons into voids left in a 3D printed concrete structure, which are then filled with conventional concrete to bond the steel to the surrounding printed structure [14–16]. Other strategies include Asprone et al. [17] that suggest using voids for anchoring external reinforcement to provide added flexibility in how the reinforcement bars are arranged, and Baz et al. [18] that place rebar directly into 3D printed concrete between print layers. However, while using conventional rebars for reinforcement in DFC benefits from the use of available low-cost construction components, they do not leverage the high degree of design freedom afforded by digital fabrication.

Some research has therefore been conducted on digital fabrication and 3D printing of the reinforcing steel itself [19–21]. Mechtcherine et al. [19] suggest 3D printing steel reinforcement for use with 3D printed concrete. This technique demonstrates a steel–concrete bonding quality similar to that of conventional steel reinforcement. However, the steel bars exhibit a 20% loss in yield stress and tensile strength compared to conventional rebars, and the time required for such fabrication is long and likely prohibitive. Although the authors do not state an average fabrication rate, they note that a waiting period of 30 s is required between 0.2 mm thick layers, meaning at least 25 min per 1 cm of reinforcing steel. Hack et al. [20] robotically assemble an external reinforcing mesh into which concrete is poured, for use as a curved wall with complex geometry. Bos et al. [21] use reinforcing steel wire that is placed simultaneously during a concrete 3D printing process, and tests the bonding efficacy. The pull-out strength of the reinforcing wire is found to be comparable to that of smooth rebar manufactured without surface deformations.

In addition to the direct application of digital fabrication for full scale structures, using 3D printed reinforcement for small scale physical models and prototypes is suggested by Del Giudice and Vassiliou [22], as this allows researchers to investigate and understand the structural behavior through easily repeatable physical models. While physical small-scale models have been used to study masonry behavior [23], and rock mechanics [24, 25], scale modelling of reinforced concrete prototypes has only been suggested as recently as 2011 [26]. As in other fields, rapid and reliable prototyping and experimental testing of construction components can help evaluate the efficacy of new design methods, or applications. With the rise in interest of DFC, scale testing of construction components is of increased relevance. However, using existing steel printing technologies, prototype models are currently restricted to small scales, e.g. in the order of 1:40 as in [22], or full structural scale.

As an alternative to 3D printing of the reinforcing steel, this paper explores the use of reinforcement that has been cut from steel plates with a waterjet cutting machine for DFC. While the practice of using steel plates to reinforce concrete structures dates back to the mid 1970s, steel plates have primarily been used externally to retrofit and stiffen existing elements through epoxy bonding to an outer surface [27]. Precision-cut steel plates have been explored in only limited capacities by engineers for applications in DFC. Recent examples include the use of laser-cut steel plates that are welded together and used as shaped form-works [28], and use by the authors and others of waterjet-cut (WC) steel plates as internal reinforcement in shaped reinforced concrete beams [29–31]. Cutting reinforcement from steel plates permits extraordinary design freedom for applications where non-uniform reinforcement may be desired. Although confined to a constant out-of-plane thickness, diverse in-plane member thicknesses, lengths, arrangements, and connectivity can be cut with high precision from a single plate (provided the plate and waterjet cutter are sufficiently large).

However, because of plate steel's smooth surface, it's bonding properties with the surrounding concrete must considered. Traditional rebar has deformations or "ribs" that allow for mechanical interlocking with the concrete, vastly improving bond strength [32]. Experimental work has shown the geometry of traditional rebar ribbing can influence the bond characteristics [33]. Thus, it may be advantageous to overlay a ribbed pattern onto WC steel plate reinforcement, to act similarly to the deformations along standard rebar. Because these ribs would only be active along one dimension of the steel, rather than surrounding the entire rebar member, consideration of how best to design the pattern is of tantamount importance. Provided the ribbing can be designed to ensure a sufficient steel–concrete bond strength, WC reinforcement offers some advantages over current steel reinforcement construction methods, particularly for reinforcing geometries of high complexity and for medium-scaled physical prototypes.

Therefore, this paper seeks to experimentally explore the effect of applying different ribbing patterns on the steel–concrete bond strength of WC plate reinforcement. Pullout tests are performed on internally reinforced concrete specimens with both conventional rebar and WC steel plates. Three different ribbing patterns are applied to the steel plate reinforcement. The maximum pullout force is recorded, and the bond strength of all tested specimens is calculated and compared. In addition, the observed formation of cracks after test completion is evaluated to suggest future strategies for improving the bond strength.

Experimental procedure

Reinforcement design and preparation

The bond strength was evaluated herein for four different reinforcing steel configurations: (i) regular ribbed rebars, and WC steel plates with ribbing patterns in the shape of (ii) isosceles triangles, (iii) semicircles, and (iv) inverse semicircles. The rebars were Grade 40 No. 6 bars with Ø19mm

(Ø 0.75 in) and a yield strength of 275.8 MPa (40 ksi) manufactured to meet ASTM A615 standards. The steel plates were 304 stainless steel of 1.27 cm (0.5 in) thickness with a yield strength of 206.8 MPa (30 ksi) meeting ASTM A276 standards. The difference in yield strength was not assumed to be impactful to the experiment, as the specimen were designed to reach steel–concrete bond failure before the steel would yield. This is discussed further in Sect. 4 with the results of the experiment.

Figure 1 shows schematics of the three WC reinforcement types and gives examples of all used reinforcement configurations. The isosceles triangles pattern has previously been used by the authors [31], while both circular patterns were added to investigate potential benefits of curvature and concrete interlocking. All WC designs had the same cross-sectional area of the standard rebar (Ø 19 mm) of 2.83 cm^2. Because the steel plates were manufactured with a thickness of 1.27 cm (0.5 in), the width of the minimum section was chosen as 2.24 cm (0.88 in). The ribbing patterns all used the same height of 0.5 cm and depth of 1.0 cm.

Cutting models were prepared in Rhino and fabricated using an OMAX CNC-controlled waterjet cutting machine. The machine works by selectively eroding stock material with a precisely targeted stream of high-pressure water mixed with an abrasive material, which in this case was Garnet sand. The stream is fixed to a 3-axis gantry system which is moved computationally according to the digital files provided by the designer. The OMAX was programmed to run at a low quality level, indicating a fast speed, low precision, and high taper cut. This setting was chosen to reduce cutting time and create a rougher cut to improve the bonding between the concrete and steel. Three samples for each of the four rebar test types were prepared, resulting in 12 reinforcement samples of which nine were digitally manufactured.

Experimental setup

This work used the test configuration in Fig. 2 to evaluate bond strength. The experimental approach was similar to the methodology in [34, 35] and evaluated in-depth by Chu et al. in [36]. A reinforcing steel member was placed inside a concrete cylinder. Vertical displacement was applied to the steel reinforcement at a constant rate of 5 mm/min (0.197 inches/min) until failure. A flat stabilizing plate at the top of the concrete cylinder holds the cylinder in place by preventing upward movement of the concrete sample. Applied force and steel displacement were measured simultaneously throughout the tests.

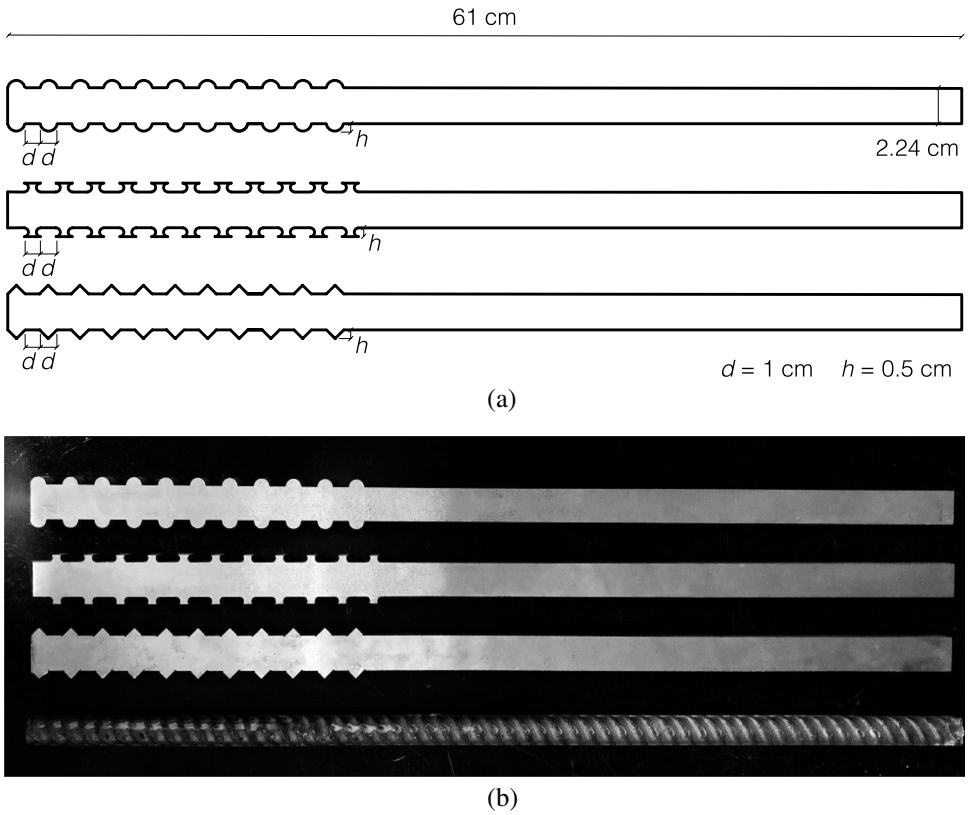

Fig. 1 (**a**) Dimensions of the plate rebar geometries, and (**b**) images of the steel reinforcement types. Top to bottom order: Circle cut, inverse semi-circle cut, triangle cut, and typical ribbed No. 6 reinforcement

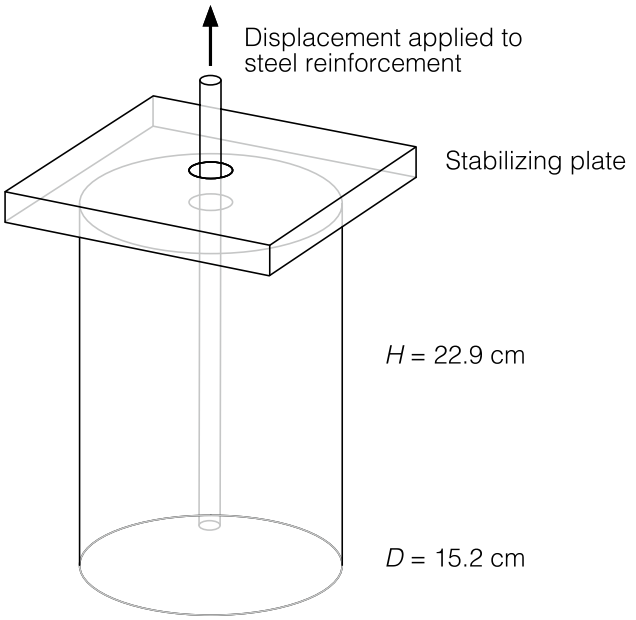

Fig. 2 Pullout test configuration

In addition to the pullout tests, uniaxial compression tests were conducted to measure the compressive strength of the concrete. A sample compression rate of 60 kN/min (13.5 kips-force/min) is used. All testing was performed on a Baldwin Universal Testing Machine.

Concrete casting

To prepare the reinforced concrete test samples, the reinforcement specimens were placed in cylinder molds and 27.6 MPa (4,000 psi) Quikrete concrete mix meeting ASTM C 387 compressive strength requirements was cast into the mold. Twelve large cylinders measuring 15.2 cm × 30.5 cm (6 in × 12 in) were used. The rebar testing molds were only filled to a height of 22.9 cm (9 in). For each sample, two equilateral triangular wooden plates of thickness 1.3 cm (0.5 in) were manufactured, whose vertices were rounded and defined by a circle of diameter 15.2 cm (6 in) (see Fig. 3). These fit snugly within the rebar test cylinder molds. Circular holes were drilled at the center of these triangles to make a tight fit around the rebar samples, holding them in place.

Two concrete batches were prepared for the experiments. Three small 10.2 cm×20.3 cm (4 in×8 in) cylindrical molds were cast from each batch to test the plain concrete strength. All rebar types were fabricated with at least one sample from each of the two concrete batches.

All samples were hydrated while curing to limit cracking. After 21 days, the samples are demolded and tested, with the bottom wood plate kept in place during the tests.

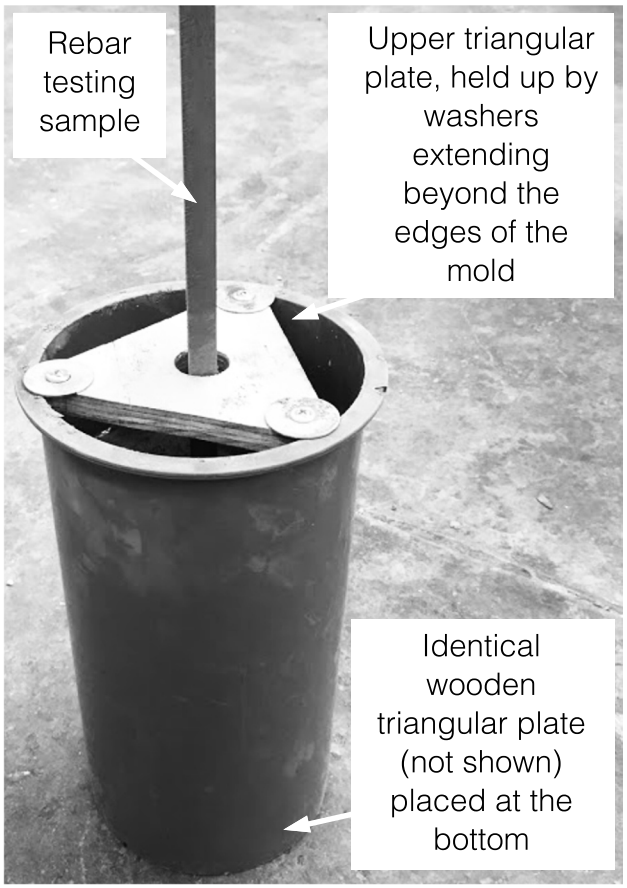

Fig. 3 Testing mold configuration for rebar samples

Calculation of bond strength

Maximum bond strength u_m of ribbed rebar has classically been calculated using the following formula [37]:

$$u_m = \frac{U}{\Sigma_o} = \frac{F}{(l)(P_s)} \tag{1}$$

where U is the force per unit length and Σ_o is the sum of the perimeters of the bars developed at a section. For this experiment, $U = {}^{F}\!/_{l}$, where F is the ultimate load at failure and l is the embedded length of the rebar, and $\Sigma_o = P_s$, where P_s is the perimeter of a section of the reinforcing bar. For typical rebar, $P_s = \pi d$, where d is the diameter of the steel. For these experiments, No 6 rebar was used, giving $P_s = \pi(19\text{ mm}) = 5.98$ cm. Because the WC samples were designed to have equal cross-sectional surface area, their perimeter is different, with $P_s = 7.08$ cm. All section areas and parameters are summarized in Table 1.

Table 1 Effective cross-sectional areas [cm^2] and cross-sectional perimeters [cm] of the four reinforcement types

	Typical	Triangular	Inverse semi-circular	Circular
Area, A_s	2.83	2.84	2.84	2.84
Perimeter, P_s	5.98	7.08	7.08	7.08

Results and discussion

Experimental results

The results of the compressive concrete tests showed that the ultimate strengths of concrete batches 1 and 2 were 33.6 MPa (4.87 ksi) and 32.4 MPa (4.70 ksi) respectively, a 4% difference in strength from each other and 21% and 17% higher than the expected strength of 27.6 MPa (4 ksi).

The results of the pullout test experiment are shown in Fig. 4 that gives the load–displacement curves for all tested samples, grouped by reinforcement type. All results show a linear elastic response followed by a rapid failure. The graphs show no indication of plateauing before failure, which suggests that none of the steel has yielded before the failure of the steel–concrete bond. Sudden dips in the force–displacement curves suggest poor bonding between the concrete and reinforcing steel, as they may indicate slippage between the concrete and rebar, or microcracking at the material interface. The specimens with standard rebar and

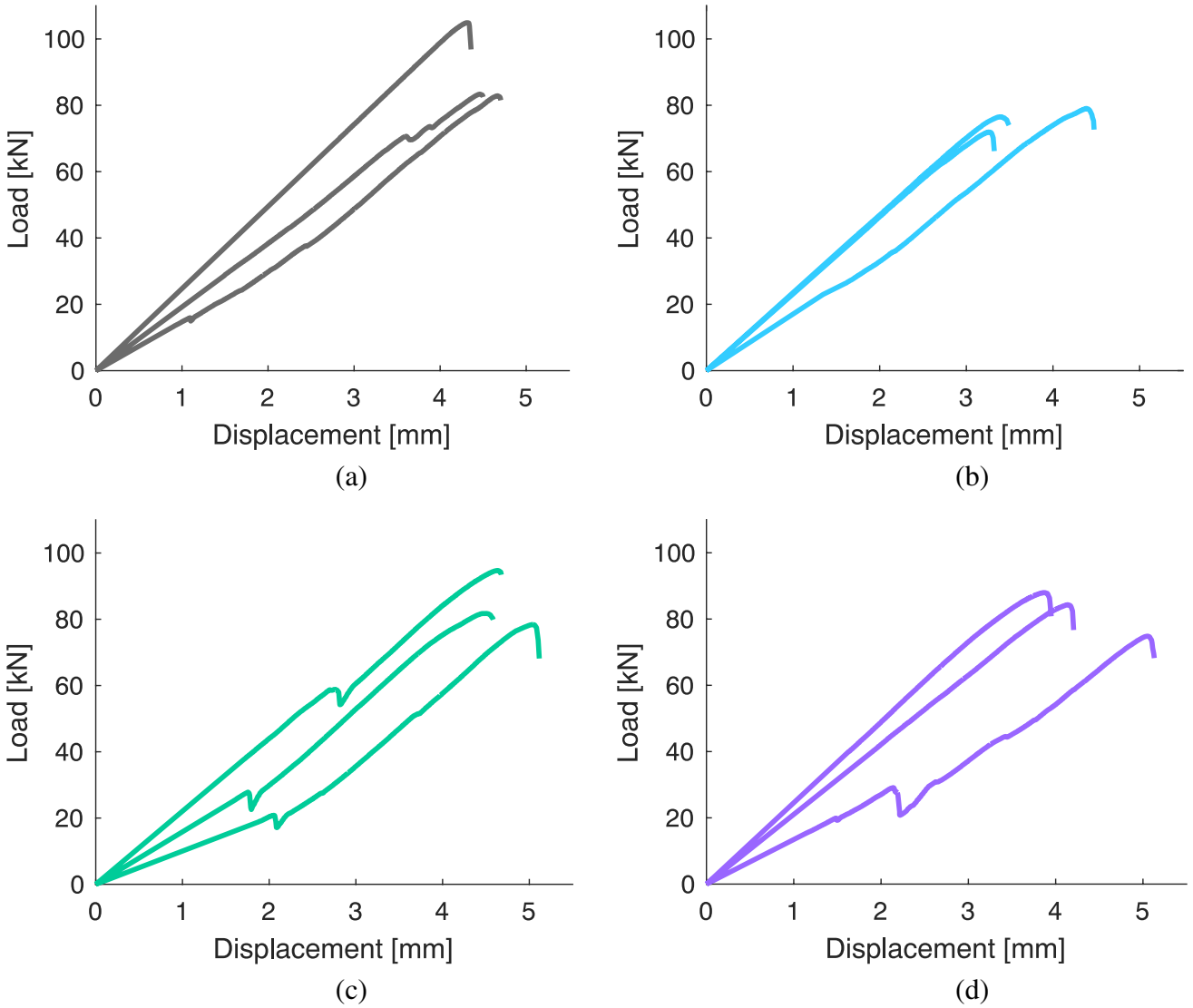

Fig. 4 Experimentally obtained load versus displacement for all pullout test samples (**a**) typical rebar; (**b**) triangular; (**c**) Inverted Semicircular; (**d**) Circular

triangle ribbings both have smoother, more linear curves when compared to the others, indicating superior bonding. No dips are observed for the specimens with WC triangular reinforcement (Fig. 4b). Similarly, almost no dips are observed for the standard rebar specimens for loads below $F = 60$ kN (13.5 kips), except one sample that exhibits a slight dip between 1 mm and 1.5 mm of displacement (Fig. 4a). Conversely, the results for the specimens with inverted semicircular and semicircular WC reinforcement both show points of more sudden dips in the range between 15 and 50% of the final strength (Fig. 4c–d).

Bond strength analysis

As discussed in Sect. 3, bond strength is usually analyzed as a pressure force MPa (Eq. (1)). However, in this experiment, the surface areas of the typical rebars is not equal to that of the WC steel. For this reason, the initial analysis will focus on the maximum force applied before failure, rather than the force per area over the steel sample. Table 2 shows the ultimate load for each sample. The standard rebar achieves the maximum average applied force. The triangular pattern samples are the weakest, with an average value of 84% to that of the standard rebar. This result is surprising, given that the force–displacement curves showed no sudden dips in any tested samples. The specimens with semicircular and inverse semicircular WC rib patterns are very close in average maximum pullout force and achieve over 90% of the standard rebar.

Table 2 Experimental values for maximum applied force [kN] before failure

Sample No	Typical	Triangular	Inverse semi-circular	Circular
1	82.9	79.1	78.4	74.8
2	83.4	72.0	81.7	84.3
3	105.0	76.5	94.7	88.0
Average	90.4	75.5	84.9	82.4

Figure 5 summarizes the information from Table 2. Although all maximum load levels are similar, it is seen that on average the typical rebar will outperform the WC reinforcement. However, all WC specimens are observed to require a relatively high pullout force and the ribbing design is seen to have a slight influence on the average performance.

As discussed in Sect. 3, the bond strength is calculated with the perimeter of the rebar's cross-section in the denominator. It is thus important to consider how the WC samples compare to typical rebar after correcting for their discrepancies in perimeter length. Figure 6 shows the experimental result averages, normalized by the results of the typical rebar pullout test. The plot also shows normalized results when samples are divided by their respective minimum perimeter. When the different perimeter size is taken into account, the relative performance of the WC samples drops. This suggests that their overall performance is improved by their higher surface area.

Bond failure

In Fig. 7, close-ups of a typical standard rebar and the WC reinforcement specimen are shown. For the purpose of these images, some concrete has been removed from the damaged specimens. In typical ribbed rebar, mechanical interlocking from the ribs works with frictional forces to generate the steel–concrete bond [32]. For the WC configuration (Fig. 7b–d), it is seen that concrete remains embedded within the grooves of the ribbing geometry, but does not remain adhered to the smooth surface of the steel. This suggests that the concrete and steel have successfully interlocked to form a mechanical bond along the deformed surfaces, but not the smooth surface. These results are consistent with experiments done by researchers such as Tirassa et al. [38], who demonstrated the importance of steel–concrete interlock for bond strength in conventional rebar, especially after concrete cracking. Figure 7a shows that this bond is intact on parts of the circumference of the ribbed rebar. More importantly, it is observed that the weakest location in the steel–concrete bond of the typical rebar specimens varies from sample

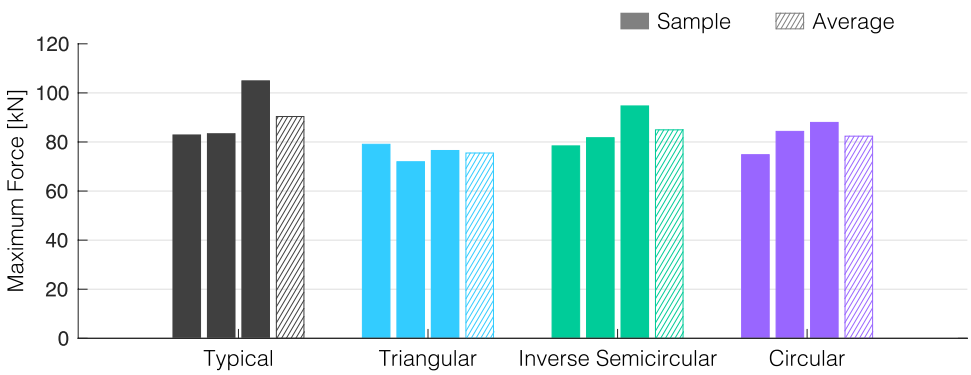

Fig. 5 Experimental results for pullout tests

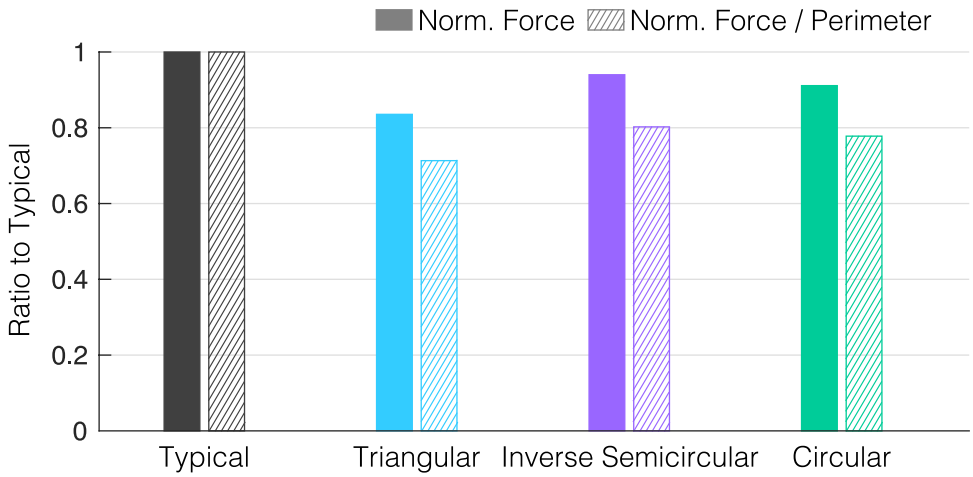

Fig. 6 Ratio of the average of each reinforcement type's maximum force and bond strength to the average bond strength of the typical rebars

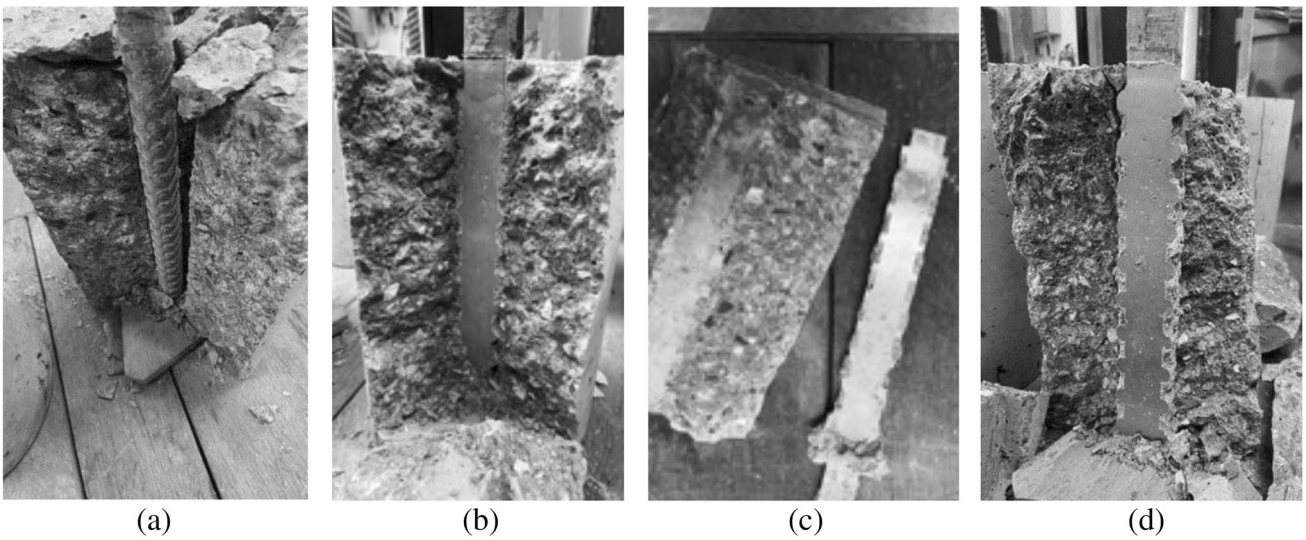

Fig. 7 Closeup view of experimental samples after failure, with (**a**) a No.6 rebar (**b**) triangular WC (**c**) Inverse Semicircle WC (**d**) circular WC samples after failure. In (**b–d**), the flat face of the reinforcement remains clean, while (**c**) and (**d**) highlight concrete embedded along the ribbed edge

to sample. This is in stark contrast to how Fig. 7b–d show that the flat face of the WC steel retains very little concrete. Despite all tested rib patterns requiring average pullout loads in the range of 84–91% that of the standard rebar, the undeformed faces of WC reinforcement seem to clearly reduce the bond performance. Potential strategies to improve the bond strength of WC reinforcement for DFC would thus benefit from addressing this issue.

Conclusion and outlook

This work has experimentally evaluated the bond performance of four different steel configurations for reinforced concrete via pullout tests. Three configurations were digitally manufactured by WC steel plates with different ribbing patterns. These designs were compared to a standard steel rebar with the same effective cross-sectional area. The results show that all tested WC specimens require pullout loads of 79%- 100% compared to that of the average standard rebar. Designs with curvature in the ribbing patterns are found to have slightly better average performance (90% and 91% for semicircular and inverse semicircular) than the triangular design (84%). Since the WC specimens in the current study had higher surface perimeters than the standard rebar, the bond strength was seen to be in the range of 4.67 – 5.25 MPa, suggesting that the increased surface area contributes to the bond capacity. Based on these results, this new method of digital fabrication of reinforcement appears viable for highly

complex structural concrete designs and/or medium scale prototyping.

From the observed cracking patterns, it is stipulated that further improvement of the steel–concrete bond can be obtained by increasing the mechanical engagement along the flat plate surface. For example, a steel plate with manufactured surface deformations could be used in future works, as such designs are readily commercially available. Other potential strategies may include the addition of welded grooves, chemical treatment, or sandblasting to create a rougher texture, and/or the addition of intermediate holes to the reinforcement. Additionally, investigations of effects of the size of the ribbing patterns as well as thickness of the WC steel plate are recommended.

Funding Open Access funding provided by the MIT Libraries

Declarations All authors certify that they have no affiliations with or involvement in any organization or entity with any financial interest or non-financial interest in the subject matter or materials discussed in this manuscript.

References

1. Buchanan C, Matilainen V-P, Salminen A, Gardner L (2017) Structural performance of additive manufactured metallic material and cross-sections. J Constr Steel Res 136:35–48. https://doi.org/10.1016/j.jcsr.2017.05.002
2. Søndergaard A, Feringa J, Stan F, Maier D (2018) Robotic abrasive wire cutting of polymerized styrene formwork systems for cost-effective realization of topology-optimized concrete structures. Constr Robot 2:81–92. https://doi.org/10.1007/s41693-018-0016-8
3. Dörfler K, Sandy T, Giftthaler M et al (2016) Mobile Robotic Brickwork. In: Reinhardt D, Saunders R, Burry J (eds) Robotic Fabrication in Architecture, Art and Design 2016. Springer International Publishing, Cham, pp 204–217
4. Wangler T, Roussel N, Bos FP et al (2019) Digital concrete: A review. Cem Concr Res 123:105780. https://doi.org/10.1016/j.cemconres.2019.105780
5. Devadass P, Dailami F, Mollica Z, Self M (2016) Robotic fabrication of non-standard material. ACADIA 2016:206–213
6. Buchanan C, Gardner L (2019) Metal 3D printing in construction: A review of methods, research, applications, opportunities and challenges. Eng Struct 180:332–348. https://doi.org/10.1016/j.engstruct.2018.11.045
7. Siddika A, Mamun MdAA, Ferdous W et al (2020) 3D-printed concrete: applications, performance, and challenges. J Sustain Cem-Based Mater 9:127–164. https://doi.org/10.1080/21650373.2019.1705199
8. Lloret E, Shahab AR, Linus M et al (2015) Complex concrete structures. Comput-Aided Des 60:40–49. https://doi.org/10.1016/j.cad.2014.02.011
9. Popescu M, Rippmann M, Liew A et al (2021) Structural design, digital fabrication and construction of the cable-net and knitted formwork of the KnitCandela concrete shell. Structures 31:1287–1299. https://doi.org/10.1016/j.istruc.2020.02.013
10. Jipa A, Dillenburger B (2021) 3D Printed formwork for concrete: State-of-the-art, opportunities, challenges, and applications. 3D Print Addit Manuf 3dp.2021.0024. https://doi.org/10.1089/3dp.2021.0024
11. Asprone D, Menna C, Bos FP et al (2018) Rethinking reinforcement for digital fabrication with concrete. Cem Concr Res 112:111–121. https://doi.org/10.1016/j.cemconres.2018.05.020
12. Gaganelis G, Mark P (2019) Downsizing weight while upsizing efficiency: An experimental approach to develop optimized ultra-light UHPC hybrid beams. Struct Concr 20:1883–1895. https://doi.org/10.1002/suco.201900215
13. Lloret-Fritschi E, Scotto F, Gramazio F et al (2019) Challenges of real-scale production with smart dynamic casting. In: Wangler T, Flatt RJ (eds) First RILEM International Conference on Concrete and Digital Fabrication – Digital Concrete 2018. Springer International Publishing, Cham, pp 299–310
14. Anton A, Bedarf P, Yoo A, Dillenburger B Concrete choreography: Prefabrication of 3D-printed columns. In: Fabricate 2020: Making Resilient Architecture. pp 286–293
15. Salet TAM, Ahmed ZY, Bos FP, Laagland HLM (2018) Design of a 3D printed concrete bridge by testing. Virtual Phys Prototyp 13:222–236. https://doi.org/10.1080/17452759.2018.1476064
16. Lim S, Buswell R, Le T, et al (2011) Development of a Viable Concrete Printing Process. Seoul, Korea
17. Asprone D, Auricchio F, Menna C, Mercuri V (2018) 3D printing of reinforced concrete elements: Technology and design approach. Constr Build Mater 165:218–231. https://doi.org/10.1016/j.conbuildmat.2018.01.018
18. Baz B, Aouad G, Leblond P, et al (2020) Mechanical assessment of concrete-steel bonding in 3D printed elements. Constr Build Mater 256. https://doi.org/10.1016/j.conbuildmat.2020.119457
19. Mechtcherine V, Grafe J, Nerella VN et al (2018) 3D-printed steel reinforcement for digital concrete construction – Manufacture, mechanical properties and bond behaviour. Constr Build Mater 179:125–137. https://doi.org/10.1016/j.conbuildmat.2018.05.202
20. Agustí-Juan I, Müller F, Hack N et al (2017) Potential benefits of digital fabrication for complex structures: Environmental assessment of a robotically fabricated concrete wall. J Clean Prod 154:330–340. https://doi.org/10.1016/j.jclepro.2017.04.002
21. Bos F, Ahmed Z, Jutinov E, Salet T (2017) Experimental exploration of metal cable as reinforcement in 3D printed concrete. Materials 10:1314. https://doi.org/10.3390/ma10111314
22. Del Giudice L, Vassiliou MF (2020) Mechanical properties of 3D printed material with binder jet technology and potential applications of additive manufacturing in seismic testing of structures. Addit Manuf 36:101714. https://doi.org/10.1016/j.addma.2020.101714
23. DeJong MJ, Vibert C (2012) Seismic response of stone masonry spires: Computational and experimental modeling. Eng Struct 40:566–574. https://doi.org/10.1016/j.engstruct.2012.03.001
24. Tian W, Han N (2017) Mechanical properties of rock specimens containing pre-existing flaws with 3D printed materials. Strain. https://doi.org/10.1111/str.12240

25. Jiang C, Zhao G-F (2015) A preliminary study of 3D printing on rock mechanics. Rock Mech Rock Eng 48:1041–1050. https://doi.org/10.1007/s00603-014-0612-y
26. Knappett JA, Reid C, Kinmond S, O'Reilly K (2011) Small-scale modeling of reinforced concrete structural elements for use in a geotechnical centrifuge. J Struct Eng 137:1263–1271. https://doi.org/10.1061/(ASCE)ST.1943-541X.0000371
27. Täljsten B (1997) Strengthening of beams by plate bonding. J Mater Civ Eng 9:206–212. https://doi.org/10.1061/(ASCE)0899-1561(1997)9:4(206)
28. Ismail MA, Mueller CT (2021) Minimizing embodied energy of reinforced concrete floor systems in developing countries through shape optimization. Eng Struct 246:112955. https://doi.org/10.1016/j.engstruct.2021.112955
29. Ismail MA, Mueller C (2019) A Platform of Design Strategies for the Optimization of Concrete Floor Systems in India. In: Cruz PJS (ed) Structures and Architecture: Bridging the Gap and Crossing Borders, 1st edn. CRC Press, pp 399–408
30. Jewett JL, Carstensen JV (2019) Experimental investigation of strut-and-tie layouts in deep RC beams designed with hybrid bilinear topology optimization. Eng Struct 197:109322. https://doi.org/10.1016/j.engstruct.2019.109322
31. Liu Y, Jewett JL, Carstensen JV (2020) Experimental investigation of topology-optimized deep reinforced concrete beams with reduced concrete volume. In: Bos F, Lucas S, Wolfs R, Salet T (eds) Second RILEM International Conference on Concrete and Digital Fabrication. Springer International Publishing, Cham
32. Nilson A, Darwin D, Dolan C (2010) Design of Concrete Structures, 14th edn. McGraw Hill, New York, NY
33. Reinhardt HW, Balázs GL (1995) Steel-concrete interfaces: experimental aspects. In: Mechanics of geomaterial interfaces, pp 255–279
34. Ganesan N, Indira PV, Sabeena MV (2014) Bond stress slip response of bars embedded in hybrid fibre reinforced high performance concrete. Constr Build Mater 50:108–115. https://doi.org/10.1016/j.conbuildmat.2013.09.032
35. Güneyisi E, Gesoğlu M, İpek S (2013) Effect of steel fiber addition and aspect ratio on bond strength of cold-bonded fly ash lightweight aggregate concretes. Constr Build Mater 47:358–365. https://doi.org/10.1016/j.conbuildmat.2013.05.059
36. Chu SH, Kwan AKH (2018) A new method for pull out test of reinforcing bars in plain and fibre reinforced concrete. Eng Struct 164:82–91. https://doi.org/10.1016/j.engstruct.2018.02.080
37. (2021) ACI 408R-03: Bond and development of straight reinforcing bars in tension
38. Tirassa M, Fernández Ruiz M, Muttoni A (2021) An interlocking approach for the rebar-to-concrete contact in bond. Mag Concr Res 73:379–393. https://doi.org/10.1680/jmacr.20.00209